5-2015

SO(8) Fermion Dynamical Symmetry in Graphene

Matthew Murphy
University of Tennessee - Knoxville, mmurph38@vols.utk.edu

SO(8) Fermion Dynamical Symmetry in Graphene

Matthew Murphy
Advised by Dr. Mike Guidry

May 5, 2015

1 Introduction

Graphene is a form of carbon consisting of a single layer of carbon atoms arrayed in a hexagonal grid, a single layer of bulk graphite. It was first isolated in 2004 by Geim and Novoselov[1] (a feat for which they won the 2010 Nobel Prize), and is thus a fairly new area of study. Graphene is of particular interest because its nearly two-dimensional structure is unique among materials. This paper explores the electronic structure of graphene under an applied magnetic field, particularly the existing SU(4) symmetry description and the new SO(8) description developed by Drs. Guidry and Wu in an upcoming paper[2], to which I have also made several contributions.

2 Basic Structure of Graphene

Each carbon atom in graphene has 4 valence electrons, 3 of which hybridize in the sp^2 manner and form σ bonds with their neighbors, and 1 of which (by convention, the electron in the p_z orbital) delocalizes and forms π bonds. To examine the dispersion relation of graphene, we first divide the hexagonal lattice into two triangular lattices, A and B, as we observe that two neighboring atoms do not have identical neigborhoods, and thus the unit cell must have a two-atom basis. This division into A and B lattices is shown in Figure 1.

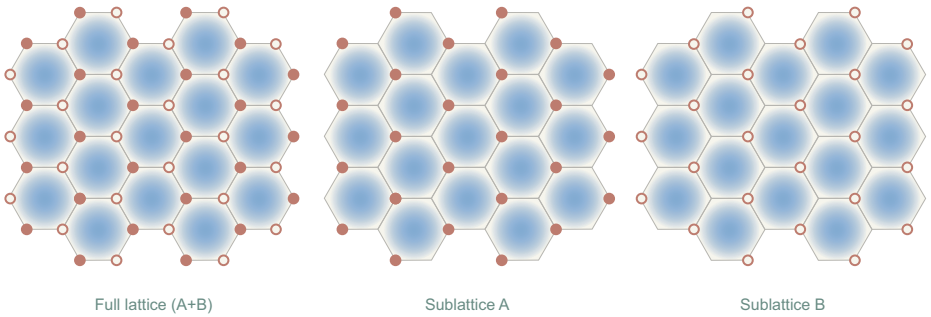

Figure 1: A and B sublattices[2]

2.1 Derivation of the Dispersion Relation

Following the method used by Goerbig[3], we will now derive the dispersion relation for graphene, which is essential to understanding its properties.

First we construct a Bravais lattice, defined by the vectors $\mathbf{a}_1 = \sqrt{3}a\mathbf{e}_x$ and $\mathbf{a}_2 = \frac{\sqrt{3}a}{2}(\mathbf{e}_x + \sqrt{3}\mathbf{e}_y)$, which can be aligned with either the A or B sublattices. Here a is the interatomic spacing (about 0.142 nm) between carbon atoms. This is shown in Figure 2 (a).

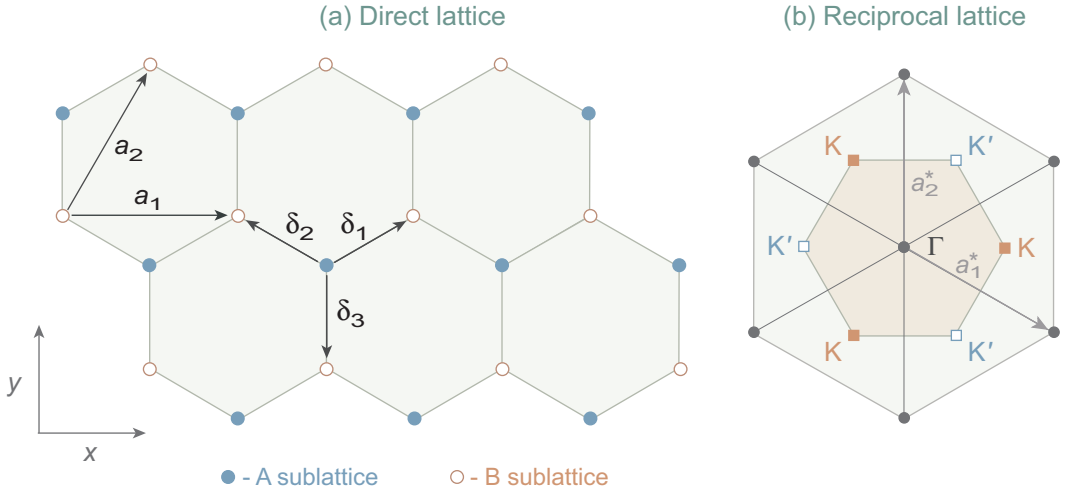

Figure 2: (a)Bravais lattice vectors a_1 and a_2 and vectors $\delta_{1,2,3}$ connecting the A sublattice to the Bravais lattice, which here is aligned to the B sublattice (b)Reciprocal lattice, showing the two sets of inequivalent lattice points K and K'.[2]

2.1.1 General Solution

As we have two atoms per unit cell, we write down a trial wave function

$$\psi_{\mathbf{k}}(\mathbf{r}) = a_{\mathbf{k}}\psi_{\mathbf{k}}^{(A)}(\mathbf{r}) + b_{\mathbf{k}}\psi_{\mathbf{k}}^{(B)}(\mathbf{r}) \tag{1}$$

where $\psi_{\mathbf{k}}^{(A)}(\mathbf{r})$ and $\psi_{\mathbf{k}}^{(B)}(\mathbf{r})$ are Bloch functions of the form

$$\boldsymbol{\psi}_{\mathbf{k}}^{(j)}(\mathbf{r}) = \sum_{\mathbf{R_l}} e^{i\mathbf{k}\cdot\mathbf{r}}\boldsymbol{\phi}^{(j)}(\mathbf{r} + \boldsymbol{\delta}_j - \mathbf{R}_l) \tag{2}$$

where j=A,B is a label for atoms on sublattices A and B, $\boldsymbol{\delta_j}$ connects the sites of the underlying (triangular) Bravais lattice to the site of the j atom in the unit cell (so if we have aligned the Bravais lattice to sublattice A, $\delta_{\mathbf{A}} = \mathbf{0}$ and $\delta_{\mathbf{B}} = -a\mathbf{e}_y$), and $\phi^{(j)}(\mathbf{r} - (\mathbf{R}_l - \delta_j))$ are the wave functions for the atomic orbitals for the j atom of the unit cell at lattice position $\mathbf{R}_l$.

Now we attempt to solve the Schrödinger equation $H\psi_{\mathbf{k}} = \epsilon_{\mathbf{k}}\psi_{\mathbf{k}}$. Left-multiplying by $\psi^*_{\mathbf{k}}$ and rewriting in matrix form gives, referring to (1),

$$(a^*_{\mathbf{k}}, b^*_{\mathbf{k}})\mathcal{H}_{\mathbf{k}}\begin{pmatrix} a_{\mathbf{k}} \\ b_{\mathbf{k}} \end{pmatrix} = \epsilon_{\mathbf{k}}(a^*_{\mathbf{k}}, b^*_{\mathbf{k}})\mathcal{S}_{\mathbf{k}}\begin{pmatrix} a_{\mathbf{k}} \\ b_{\mathbf{k}} \end{pmatrix} \tag{3}$$

where $\mathcal{H}_{\mathbf{k}}$ is a Hermitian Hamiltonian matrix with entries $\mathcal{H}_{\mathbf{k}(i,j)} = \psi^{(i)*}_{\mathbf{k}} H \psi^{(j)}_{\mathbf{k}}$ and $\mathcal{S}_{\mathbf{k}}$ is the (also Hermitian) overlap matrix with elements $\mathcal{S}_{\mathbf{k}(i,j)} = \psi^{(i)*}_{\mathbf{k}}\psi^{(j)}_{\mathbf{k}}$, which accounts for the fact that the trial wavefunctions are not necessarily orthogonal. Then we obtain the eigenvalues $\epsilon^{\lambda}_{\mathbf{k}}$ of the Hamiltonian from the equation

$$|\mathcal{H}_{\mathbf{k}} - \epsilon^{\lambda}_{\mathbf{k}}\mathcal{S}_{\mathbf{k}}| = 0 \tag{4}$$

In order to solve this, we first define the matrices

$$s^{ij}_{\mathbf{k}} \equiv \sum_{\mathbf{R_l}} e^{i\mathbf{k}\cdot\mathbf{R_l}} \int \phi^{(i)*}(\mathbf{r})\phi^{(j)}(\mathbf{r} + \delta_{ij} - \mathbf{R_l})d^2r \tag{5}$$

which gives the total overlap between atoms at sites i and j in the unit cell, where $\delta_{ij} = \delta_j - \delta_i$, and

$$t^{ij}_{\mathbf{k}} \equiv \sum_{\mathbf{R_l}} e^{i\mathbf{k}\cdot\mathbf{R_l}} \int \phi^{(i)*}(\mathbf{r})\Delta V\phi^{(j)}(\mathbf{r} + \delta_{ij} - \mathbf{R_l})d^2r \tag{6}$$

which is the hopping matrix defining the ability of an electron to move from lattice site i to site j. We then rewrite the Hamiltonian : $\mathcal{H}^{ij}_{\mathbf{k}} = N(\epsilon^{(j)}s^{ij}_{\mathbf{k}} + t^{ij}_{\mathbf{k}})$, which essentially divides it into a portion H^a based on the atomic orbitals, which defines an on-site energy $\epsilon^{(j)}$, and a perturbation ΔV which arises from the interaction with the rest of the lattice. Noticing now that $s^{ij}_{\mathbf{k}} = \frac{\mathcal{S}^{ij}_{\mathbf{k}}}{N}$, we can rewrite our eigenvalue equation as

$$|t^{ij}_{\mathbf{k}} - (\epsilon^{\lambda}_{\mathbf{k}} - \epsilon^{(j)})s^{ij}_{\mathbf{k}}| = 0 \tag{7}$$

If, as is the case with graphene, all sublattices have electrons in the same atomic orbitals, $\epsilon^{(j)}$ is a constant ϵ_0, which is physically irrelevant, as it provides only a constant shift in the energy bands.[3]

2.1.2 Specific Solution for Graphene in the Tight-Binding Approximation

To utilize these results in the case of graphene, we shall fix the Bravais lattice to the A sublattice, and then we have $\delta_B = \delta_3$ from Figure 2 (a). This is illustrated in Figure 3. In the tight-binding approximation, we consider only the nearest-neighbor (NN) hopping and overlap interactions, and the next-nearest-neighbor (NNN) hopping interaction. The magnitude of the NN hopping amplitude is given by

$$t = \int \phi^{A*}(\mathbf{r})\Delta V\phi^{B}(\mathbf{r} + \delta_3)d^2r \tag{8}$$

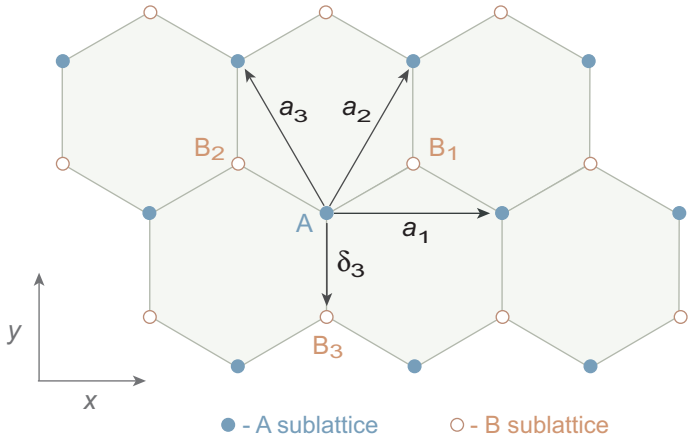

Figure 3: Important tight-binding vectors for the graphene lattice.[4]

and for NNN hopping, it is

$$t_{NNN} = \int \phi^{A*} \Delta V \phi^{A}(\mathbf{r} + \mathbf{a}_1) d^2 r \tag{9}$$

The magnitude of the off-diagonal elements of the NN overlap matrix are

$$s = \int \phi^{A*}(\mathbf{r}) \phi^{B}(\mathbf{r} + \delta_3) d^2 r \tag{10}$$

(the diagonal elements are 1 due to the normalization of the atomic orbital wave functions). When we consider the total phase, however, we see that only one of the NN sites, B_3 does not contribute to the phase, because it is described by the same lattice vector as A, except shifted by δ_3, while the other two NN points, B_1 and B_2 are shifted by $\mathbf{a}_2$ and $\mathbf{a}_3$, respectively. Thus we introduce the quantity

$$\gamma_{\mathbf{k}} \equiv 1 + e^{i\mathbf{k}\cdot\mathbf{a}_2} + e^{i\mathbf{k}\cdot\mathbf{a}_3} \tag{11}$$

so we can write the off-diagonal elements of the hopping matrix as $t_{\mathbf{k}}^{AB} = t\gamma_{\mathbf{k}}^{*} = (t_{\mathbf{k}}^{BA})^{*}$, and similarly, the off-diagonal elements of the overlap matrix are $s_{\mathbf{k}}^{AB} = s\gamma_{\mathbf{k}}^{*} = (s_{\mathbf{k}}^{BA})^{*}$. We also arrive at the diagonal elements of the hopping matrix from the NNN correlations: $t_{\mathbf{k}}^{AA} = t_{\mathbf{k}}^{BB} = t_{NNN}(|\gamma_{\mathbf{k}}|^2 - 3)$. Then, eliminating the constant $\epsilon^{(j)} = \epsilon_0$ term from Equation 7, we can finally determine the energy levels of graphene according to the solution to

$$\begin{vmatrix} t_{\mathbf{k}}^{AA} - \epsilon_{\mathbf{k}} & (t - s\epsilon_{\mathbf{k}})\gamma_{\mathbf{k}}^{*} \\ (t - s\epsilon_{\mathbf{k}})\gamma_{\mathbf{k}} & t_{\mathbf{k}}^{AA} - \epsilon_{\mathbf{k}} \end{vmatrix} = 0 \tag{12}$$

with some amount of work, it can be shown that this gives two eigenvalues:

$$\epsilon_{\mathbf{k}}^{\lambda} = \frac{t_{\mathbf{k}}^{AA} + \lambda t|\gamma_{\mathbf{k}}|}{1 + \lambda s|\gamma_{\mathbf{k}}|} \qquad \lambda = \pm 1 \tag{13}$$

We now make the approximations $s \ll 1$ and $t_{NNN} \ll t$ and this expression simplifies to

$$\epsilon_{\mathbf{k}}^{\lambda} \approx t_{\mathbf{k}}^{AA} + \lambda t|\gamma_{\mathbf{k}}| - st|\gamma_{\mathbf{k}}|^2 = (t_{NNN} - st)|\gamma_{\mathbf{k}}|^2 + \lambda t|\gamma_{\mathbf{k}}| - 3t_{NNN} \tag{14}$$

Neglecting the constant of $-3t_{NNN}$, and doing the explicit multiplication of $|\gamma_{\mathbf{k}}|^2$ gives

$$\epsilon_{\mathbf{k}}^{\lambda} \approx (t_{NNN} - st)\left(3 + 2\sum_{i=1}^{3}\cos\left(\mathbf{k}\cdot\mathbf{a}_i\right)\right) + \lambda t\sqrt{3 + 2\sum_{i=1}^{3}\cos\left(\mathbf{k}\cdot\mathbf{a}_i\right)} \tag{15}$$

with the vectors

$$\mathbf{a}_1 = \sqrt{3}a\mathbf{e}_x \tag{16}$$

$$\mathbf{a}_2 = \frac{\sqrt{3}a}{2}(\mathbf{e}_x + \sqrt{3}\mathbf{e}_y) \tag{17}$$

$$\mathbf{a}_3 = \frac{\sqrt{3}a}{2}(-\mathbf{e}_x + \sqrt{3}\mathbf{e}_y) \tag{18}$$

More advanced numerical calculation of the band structure and experimental spectroscopic results indicate that reasonable values for these constants are $t \approx -3$ eV and $t_{NNN} - st \approx -0.3$ eV. The following figure was produced in Matlab using these values to illustrate this relation.

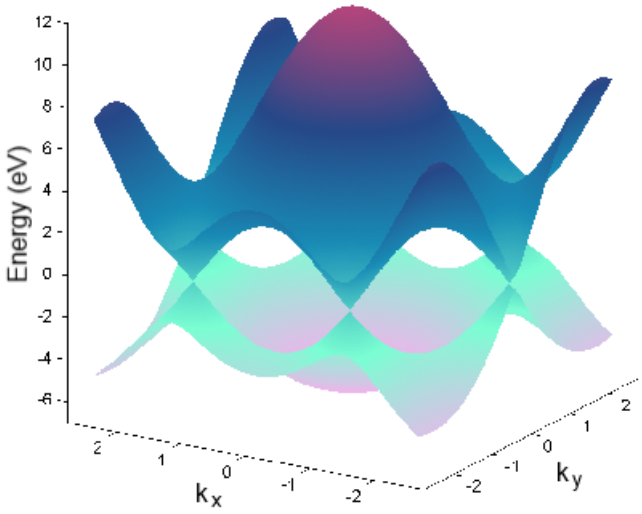

Figure 4: Dispersion relation for graphene.

2.2 Interpreting the dispersion relation

The bottom surface on the graph above corresponds to $\lambda = -1$ and the upper surface corresponds to $\lambda = +1$. As we have already noted, each carbon atom in the lattice

contributes one electron to the band structure, so these electrons fill exactly the $\lambda = -1$, or valence, band, while the $\lambda = +1$ band is called the conduction band. Essential in the study of materials is the knowledge of the separation between these two bands, known as the band gap, and the way the electrons fill this band structure. In the case of graphene, this structure is particularly interesting. Instead of having a finite gap between the valence and conduction bands, they come together in a linear fashion at a number of points, known as Dirac points, illustrated in more detail below.

Figure 5: Close-up of a Dirac point in graphene

Near these Dirac points, where the energy varies linearly with momentum, the electrons act as if they were massless and relativistic; that is, rather than obeying a non-relativistic Schrödinger equation, they obey a Dirac equation, with the Fermi velocity playing the part of the speed of light. As in the case of the direct hexagonal lattice, the reciprocal lattice is also composed of two sets of inequivalent Dirac points, which we will label as K and K'. This represents another degree of freedom for the electons, referred to as *valley isospin*.

3 Graphene in a Magnetic Field: The Hall Effect

When a thin current-carrying layer of a material is placed in a magnetic field, a voltage is created perpendicular to the direction of the current; this phenomenon is referred to as the Hall Effect after its discoverer, Edwin Hall. Classically, this is caused by the Lorentz force acting on the charges as they move through the magnetic field, and, depending on the material, has a particular Hall resistivity (and thus a Hall conductance). It has been shown, in fact, that this Hall conductance is quantized in multiples of $\frac{e^2}{h}$, either as an integer multiple (the integer quantum Hall effect[5]) or as some fractional multiple (the fractional quantum Hall effect[6]). Because graphene is the ideal example of a thin-layer material, an understanding of how a graphene layer reacts in a magnetic field may lead to deeper insights into the quantum Hall effect.

3.1 Quantization and Landau Levels

To understand the quantum Hall effect, first we must understand the set of quantized energy levels that are created when a thin material is placed in a magnetic field. If we have a system of non-interacting particles confined to the $x-y$ plane in an area $A = L_x L_y$ and apply a magnetic field $B = B\mathbf{e}_z$, then the Hamiltonian is[7]

$$\hat{H} = \frac{1}{2m}\left(\hat{p} - \frac{qB}{c}\hat{A}\right)^2, \tag{19}$$

where $\hat{A}$ is the electromagnetic vector potential. We choose the Landau gauge, $\hat{A} = Bx\mathbf{e}_y$, which gives

$$\hat{H} = \frac{\hat{p}_x^2}{2m} + \frac{1}{2m}\left(\hat{p}_y - \frac{qB\hat{x}}{c}\right)^2. \tag{20}$$

Since $\hat{y}$ does not appear in the Hamiltonian, $[\hat{H}, \hat{p}_y] = 0$, and we can replace $\hat{p}_y$ by its eigenvalues $\hbar k_y$, and additionally, making the substitution $\omega_c = \frac{qB}{mc}$ gives

$$\hat{H} = \frac{\hat{p}_x^2}{2m} + \frac{1}{2}m\omega_c^2\left(\hat{x} - \frac{\hbar k_y}{m\omega_c}\right)^2. \tag{21}$$

This is exactly the equation for a one-dimensional quantum harmonic oscillator with frequency ω_c, shifted on the x-axis by an amount $\frac{\hbar k_y}{m\omega_c}$, so it has the same energy eigenvalues,

$$E = \hbar\omega_c\left(n + \frac{1}{2}\right),\ n \geq 0.$$

As these energy levels, called Landau levels, do not depend on k_y, they are highly degenerate under sufficiently strong magnetic fields. As the magnetic field increases, the separation between levels also increases, so that eventually all but a few of the Landau levels are above the Fermi energy, and all of the electrons reside in these few Landau levels.

In the gaps between Landau levels, electrons do not change energy as the magnetic field increases, and we observe the integer quantum Hall effect. The fractional quantum Hall effect occurs due to the correlations between electrons when a Landau level is partially filled.

3.2 The Quantum Hall Effect in Graphene

In general, the quantum Hall conductance is given by

$$\sigma_{xy} = \frac{\nu e^2}{h}, \tag{22}$$

where ν is a filling factor. Clearly, for a typical conductor, the integer quantum Hall effect is represented by the integer values of ν, and the fractional effect by fractional values. In graphene, however, the situation is somewhat different. First, each energy,

even in the absence of a magnetic field, has a four-fold degeneracy represented by the two possible spin states and the two possible valley isospin states. Secondly, the electrons behave like massless relativistic particles in graphene, unlike in metals. The effect of this is that the filling factors corresponding to the integer quantum Hall effect in graphene have been observed to be [8, 9]

$$\nu = 4\left(n + \tfrac{1}{2}\right) = \pm 2, \pm 6, \pm 10 \ldots .$$

Here the factor of four comes from the four-fold degeneracy within the Landau levels, and the $\frac{1}{2}$ comes from a Berry phase associated with the $n = 0$ state for massless fermions.[9, 10]

In addition to these integer quantum Hall states, additional states have been observed[11, 12, 13] at filling factors $\nu = 0, \pm 1, \pm 4$, and $\nu = {}^{1}/_{3}, {}^{2}/_{3}, {}^{4}/_{3}$. Because these states do not occur due to complete filling of the Landau levels, they correspond to the "fractional" quantum Hall effect, although the filling factors are not necessarily fractional. In this paper we will develop a symmetry language for understanding the correlations present in these fractional quantum Hall states.

4 Developing an SU(4) Symmetry

In this section we will examine a model known as quantum Hall ferromagnetism, which incorporates the 4 spin-valley isospin degrees of freedom into an SU(4) symmetry representation. The assumptions made in this model to assure that the spin-isospin states are actually degenerate are:

1. Any mixing caused by electrons transitioning between Landau levels is negligible.
2. Perturbations within a Landau level are small.

4.1 Spin and Isospin operators

To develop this model, we begin with the standard Pauli spin matrices:

$$\sigma_x = \begin{pmatrix} 0 & 1 \\ 1 & 0 \end{pmatrix}, \ \sigma_y = \begin{pmatrix} 0 & -i \\ i & 0 \end{pmatrix}, \ \sigma_z = \begin{pmatrix} 1 & 0 \\ 0 & -1 \end{pmatrix}, \tag{23}$$

which obey the commutation relation

$$\left[\frac{\sigma_i}{2}, \frac{\sigma_j}{2}\right] = i\varepsilon_{ijk}\frac{\sigma_k}{2}, \tag{24}$$

where ε_{ijk} is the completely antisymmetric tensor of rank three, that is, it changes sign under any exchange of two indices, and is zero if any index is repeated. With this commutator acting as the Lie bracket, these matrices (after multiplication by i) act as the generators of the SU(2) Lie algebra, which is the set of 2×2 anti-Hermitian matrices with trace 0. These spin matrices operate on a basis of spin states

$$|\uparrow\rangle = \begin{pmatrix} 1 \\ 0 \end{pmatrix} \quad |\downarrow\rangle = \begin{pmatrix} 0 \\ 1 \end{pmatrix}. \tag{25}$$

If we multiply explicitly, these operators give

$$\begin{array}{lll} \sigma_x|\uparrow\rangle = |\downarrow\rangle & \sigma_y|\uparrow\rangle = i|\downarrow\rangle & \sigma_z|\uparrow\rangle = |\uparrow\rangle \\ \sigma_x|\downarrow\rangle = |\uparrow\rangle & \sigma_y|\downarrow\rangle = -i|\uparrow\rangle & \sigma_z|\downarrow\rangle = -|\downarrow\rangle. \end{array} \tag{26}$$

If we instead choose the representation

$$\begin{aligned} \sigma_+ &\equiv \tfrac{1}{2}(\sigma_x + i\sigma_y) = \begin{pmatrix} 0 & 1 \\ 0 & 0 \end{pmatrix} \\ \sigma_- &\equiv \tfrac{1}{2}(\sigma_x - i\sigma_y) = \begin{pmatrix} 0 & 0 \\ 1 & 0 \end{pmatrix} \\ \sigma_0 &\equiv \sigma_z = \begin{pmatrix} 1 & 0 \\ 0 & -1 \end{pmatrix} \end{aligned} \tag{27}$$

we obtain

$$\begin{array}{lll} \sigma_+|\uparrow\rangle = 0 & \sigma_-|\uparrow\rangle = |\downarrow\rangle & \sigma_0|\uparrow\rangle = |\uparrow\rangle \\ \sigma_+|\downarrow\rangle = |\uparrow\rangle & \sigma_-|\downarrow\rangle = 0 & \sigma_0|\downarrow\rangle = -|\downarrow\rangle. \end{array} \tag{28}$$

Now σ_+ acts as a raising operator, σ_- is a lowering operator, and σ_0 is again just σ_z. Now the commutation relations are

$$[\sigma_+, \sigma_-] = \sigma_0 \quad [\sigma_0, \sigma_\pm] = \pm 2\sigma_\pm. \tag{29}$$

Now we additionally introduce the analagous valley isospin matrices

$$\tau_x = \begin{pmatrix} 0 & 1 \\ 1 & 0 \end{pmatrix},\ \tau_y = \begin{pmatrix} 0 & -i \\ i & 0 \end{pmatrix},\ \tau_z = \begin{pmatrix} 1 & 0 \\ 0 & -1 \end{pmatrix}, \tag{30}$$

which act on the valley isospinor basis

$$|K\rangle = \begin{pmatrix} 1 \\ 0 \end{pmatrix} \quad |K'\rangle = \begin{pmatrix} 0 \\ 1 \end{pmatrix}, \tag{31}$$

and which we can also discuss in terms of raising and lowering operators

$$\begin{aligned} \tau_+ &\equiv \tfrac{1}{2}(\tau_x + i\tau_y) = \begin{pmatrix} 0 & 1 \\ 0 & 0 \end{pmatrix} \\ \tau_- &\equiv \tfrac{1}{2}(\tau_x - i\tau_y) = \begin{pmatrix} 0 & 0 \\ 1 & 0 \end{pmatrix} \\ \tau_0 &\equiv \tau_z = \begin{pmatrix} 1 & 0 \\ 0 & -1 \end{pmatrix}. \end{aligned} \tag{32}$$

4.2 Low-Energy Hamiltonian

In the regime we are considering, the primary energy scales are that of the Landau level separation and the Coulomb elecron repulsion, so we make the assumption that electrons do not transition between Landau levels, and within a Landau level, the primary interactions are Coulombic. As proposed in reference [14], we use the Hamiltonian

$$H = H_C + H_V + H_Z, \tag{33}$$

where H_C is the energy from the Coulomb interaction

$$H_C = \frac{1}{2}\sum_{i\neq j}\frac{e^2}{\varepsilon|\mathbf{r}_i - \mathbf{r}_j|}, \tag{34}$$

H_Z is the energy from the Zeeman effect,

$$H_Z = -\mu_B B\sum_i \sigma_z^i, \tag{35}$$

and H_V results from short-range valley-dependent interactions

$$H_V = \frac{1}{2}\sum_{i\neq j}[g_z\tau_z^i\tau_z^j + g_\perp(\tau_x^i\tau_x^j + \tau_y^i\tau_y^j)]\delta(\mathbf{r}_i - \mathbf{r}_j). \tag{36}$$

In the above equations, z is chosen to be aligned with the magnetic field B, the σ_α operate on the electronic spin, the τ_α operate on the valley isospin, and g_z and $g_\perp$ are coupling constants. The $\delta(\mathbf{r}_i - \mathbf{r}_j)$ term in H_V is nonzero only if $\mathbf{r}_i = \mathbf{r}_j$, indicating the short-range nature of the interaction.

4.3 Overall Symmetry

We now introduce the following operators, with $\alpha = x, y, z$ and $\beta = x, y$:

$$\begin{aligned} \mathcal{S}_\alpha &= \frac{1}{2}\sum_i \sigma_\alpha^i \qquad T_\alpha = \frac{1}{2}\sum_i \tau_\alpha^i \\ N_\alpha &= \frac{1}{2}\sum_i \tau_z^i\sigma_\alpha^i \quad \Pi_{\alpha\beta} = \frac{1}{2}\sum_i \tau_\beta^i\sigma_\alpha^i. \end{aligned} \tag{37}$$

This set of 15 operators is closed under commutation, forming an SU(4) Lie algebra. The $\mathcal{S}_\alpha$ represent the total spin of the system, and T_α represent the total valley isospin. In the n=0 Landau level, because it occurs at the Fermi energy at the points of the Dirac cones, there is an equivalence between the sublattice and the valley isospin degrees of freedom. Thus, the N_α measure the difference in spin between the A and B sublattices. The $\Pi_{\alpha\beta}$ couple the spin and the valley isospin as will be discussed below. All of these operators also commute with H_C, so if the contributions from H_V and H_Z are small, the system displays approximate SU(4) symmetry.

4.4 Symmetry breaking in the SU(4) model

When either H_V or H_Z fails to be negligible, however, the system experiences symmetry breaking and displays a lower degree of symmetry. If contributions from H_V break the symmetry, then in general the Hamiltonian could fail to commute with T_α, N_α, or $\Pi_{\alpha\beta}$, and if contributions from H_Z break the symmetry, the Hamiltonian will fail to commute with $\mathcal{S}_\alpha$, N_α, and $\Pi_{\alpha\beta}$. There have been four main cases of symmetry breaking identified [14, 15], related to the possible values of g_z and $g_\perp$ breaking the valley isospin symmetry, and then nonzero H_Z breaking the spin symmetry.

4.4.1 Case 1: $g_z \neq g_\perp \neq 0$

In this, most general, case, the valley isospin symmetry is completely broken and we see the symmetry chain

$$SU(4) \supset SU(2)_S \times U(1)_V \supset U(1)_S \times U(1)_V.$$

Here $SU(2)_S$ refers to the global spin symmetry after isospin symmetry is broken, and $U(1)_V$ and $U(1)_S$ represent the conservation of the z-components of isospin and spin, respectively. The first subalgebra thus is generated only by $\mathcal{S}_\alpha$ and T_z, and the second by T_z and $\mathcal{S}_z$.

4.4.2 Case 2: $g_z \neq 0, g_\perp = 0$

In this case, H_V fails to commute with the operators $\Pi_{\alpha\beta}$, but still commutes with the N_α, and we obtain the symmetry chain

$$SU(4) \supset SU(2)_S^K \times SU(2)_S^{K'} \times U(1)_V \supset U(1)_S^K \times U(1)_S^{K'} \times U(1)_V.$$

Here $SU(2)_S^K$ and $SU(2)_S^{K'}$ represent total spin conservation independently on the K and K' sublattices, a stronger condition than we observed in Case 1. Again, the introduction of the Zeeman term breaks this symmetry, and only the z-components of the spin on each sublattice are conserved.

4.4.3 Case 3: $g_z = g_\perp \neq 0$

In this case, the Hamiltonian H_V still commutes with the total isospin operators T_α, but fails to commute with the N_α and $\Pi_{\alpha\beta}$ operators. Then we obtain the symmetry chain

$$SU(4) \supset SU(2)_V \times SU(2)_S \supset SU(2)_V \times U(1)_S,$$

where both spin and isospin are conserved in the first subalgebra, and spin symmetry as usual is broken to $U(1)$ by the Zeeman term.

4.4.4 Case 4: $g_z = -g_\perp \neq 0$

In this case, H_V commutes with the six $\Pi_{\alpha\beta}$ operators and T_z, so along with the three $\mathcal{S}_\alpha$, these 10 operators generate a SO(5) subgroup:

$$SU(4) \supset SO(5) \supset U(1)_S \times SU(2)_z,$$

which is then broken by the H_Z term to conserve separately the z-components of spin and of total isospin.

The use of these broken symmetry states to describe the response of graphene to an applied magnetic field field is a powerful notion that we shall see reflected later in our other description of possible quantum Hall states.

5 Fermion Dynamical Symmetries

Now we will turn to a different way of describing the symmetries present in graphene, generated using the langauge of second quantization, consisting of operators which create or annihilate particles in particular states.[1]

5.1 Symmetry Generators

To begin expressing the possible states of graphene in this new language, we first, for simplicity, make the assumption that we are operating within a single degenerate Landau level. Then we introduce the operators $c^\dagger_{\tau\sigma m_k}$ and $c_{\tau\sigma m_k}$, which, respectively, create and annihilate an electron in the state denoted by $\tau\sigma m_k$, where $\tau = +, -$ corresponds to the isospin valleys K and K', $\sigma = \uparrow, \downarrow$ corresponds to the spin polarization, and m_k distinguishes between the degeneracies in the Landau level (as derived above in the Landau gauge, this would be k_y). These operators obey the anticommutator for fermions:

$$\begin{gathered}\{c_\alpha, c^\dagger_\beta\} \equiv c_\alpha c^\dagger_\beta + c^\dagger_\beta c_\alpha = \delta_{\alpha\beta} \\ \{c^\dagger_\alpha, c^\dagger_\beta\} = \{c_\alpha, c_\beta\} = 0,\end{gathered} \tag{38}$$

where α and β are labels for arbitrary states. For ease of notation, we introduce labels a for the four possible (σ, τ) states, as follows:

τ	σ	a
$+$	$\uparrow$	1
$+$	$\downarrow$	2
$-$	$\uparrow$	3
$-$	$\downarrow$	4

(39)

Now we introduce the 16 pair-creation operators $A^\dagger_{ab}$, where a and b are 1, 2, 3, or 4, in correspondence with the above table, which create a pair of electrons, one in state a and the other in state b, with their total momentum m_k coupled to zero:

$$A^\dagger_{ab} = \sum_{m_k} c^\dagger_{am_k} c^\dagger_{b-m_k}. \tag{40}$$

We also have the Hermitian conjugates of these operators, A_{ab}, which annihilate a pair of electrons in a similar manner. In order to obey the Pauli principle, we cannot use the operators of the form $A^\dagger_{aa}$, which would result in two fermions occupying the same state. Additionally, because of the antisymmetrization requirement that $c^\dagger_\alpha c^\dagger_\beta = -c^\dagger_\beta c^\dagger_\alpha$, we observe that $A^\dagger_{ab} = -A^\dagger_{ba}$, so only half of the pair-creation operators are actually linearly independent (and the same applies to their Hermitian conjugates). This leaves us with 12 pair-creation and pair-annihilation operators.

[1] Sections 5-7 very heavily reference [2].

Next, we also introduce 16 particle-hole operators B_{ab}, which create a particle in state a and a hole in state b.

$$B_{ab} = \sum_{m_k} c^\dagger_{am_k} c_{bm_k} - \frac{1}{4}\delta_{ab}\Omega, \tag{41}$$

where Ω is the total degeneracy of states within the single Landau level, which depends on the applied magnetic field B, and is necessary when $a = b$ because the number operator $n_\alpha = c^\dagger_\alpha c_\alpha$ counts the number of electrons in the state α. Now, among these 28 total pair-creation/annihilation and pair-hole creation operators $A^\dagger_{ab}$, A_{ab}, and B_{ab}, the commutators can be shown to be as follows:

$$\begin{aligned}
\left[A_{ab}, A^\dagger_{cd}\right] &= -\delta_{ac}B_{db} - \delta_{bd}B_{ca} + \delta_{ad}B_{cb} + \delta_{bc}B_{da} \\
\left[B_{ab}, B_{cd}\right] &= \delta_{bc}B_{ad} - \delta_{ad}B_{cb} \\
\left[B_{ab}, A^\dagger_{cd}\right] &= \delta_{bc}A^\dagger_{ad} + \delta_{bd}A^\dagger_{ca} \\
\left[B_{ab}, A_{cd}\right] &= -\delta_{ac}A_{bd} - \delta_{ad}A_{cb}
\end{aligned} \tag{42}$$

These commutation relations are, in fact, the same as those for the generators of an SO(8) Lie algebra, the language which we shall now use to describe the symmetries of these quantum Hall states in graphene.

5.2 Recovering SU(4) Symmetry

In order to relate this symmetry to previous work, we first seek to recover the SU(4) model used previously as a subalgebra of the new SO(8) model. We write the generators of the SU(4) Lie algebra using creation and annihilation operators in the following way:

$$\begin{aligned}
\mathcal{S}_\alpha &= \tfrac{1}{2}\sum_{m_k}\sum_{\tau\sigma\sigma'} \langle\sigma'|\sigma_\alpha|\sigma\rangle c^\dagger_{\tau\sigma' m_k} c_{\tau\sigma m_k} \\
T_\alpha &= \tfrac{1}{2}\sum_{m_k}\sum_{\tau\tau'\sigma} \langle\tau'|\tau_\alpha|\tau\rangle c^\dagger_{\tau'\sigma m_k} c_{\tau\sigma m_k} \\
N_\alpha &= \tfrac{1}{2}\sum_{m_k}\sum_{\tau\sigma\sigma'} \langle\tau|\tau_z|\tau\rangle\langle\sigma'|\sigma_\alpha|\sigma\rangle c^\dagger_{\tau\sigma' m_k} c_{\tau\sigma m_k} \\
\Pi_{\alpha\beta} &= \tfrac{1}{2}\sum_{m_k}\sum_{\tau\tau'\sigma\sigma'} \langle\tau'|\tau_\beta|\tau\rangle\langle\sigma'|\sigma_\alpha|\sigma\rangle c^\dagger_{\tau'\sigma' m_k} c_{\tau\sigma m_k},
\end{aligned} \tag{43}$$

where α is x, y, or z, and β is x or y, σ takes the values $\uparrow$ or $\downarrow$, and τ takes the values $+$ or $-$. Taking for example the total spin operators $\mathcal{S}$, this expression represents adding up, across all degeneracies m_k in the Landau level and both isospin degeneracies τ, the total possible spin of a particle-hole pair. These operators can all be calculated explicitly, and give a linear combination of the B_{ab}. One example of such a calculation for N_y is shown

below.

$$\begin{aligned} N_y &= \tfrac{1}{2}\sum_{m_k}\sum_{\tau\sigma\sigma'}\langle\tau|\tau_z|\tau\rangle\langle\sigma'|\sigma_y|\sigma\rangle c^\dagger_{\tau\sigma' m_k}c_{\tau\sigma m_k} \\ &= \tfrac{1}{2}\sum_{m_k}\sum_{\tau}\langle\tau|\tau_z|\tau\rangle\left(-ic^\dagger_{\tau\uparrow m_k}c_{\tau\downarrow m_k}+ic^\dagger_{\tau\downarrow m_k}c_{\tau\uparrow m_k}\right) \\ &= \tfrac{1}{2}\sum_{m_k}\left(-ic^\dagger_{+\uparrow m_k}c_{+\downarrow m_k}+ic^\dagger_{+\downarrow m_k}c_{+\uparrow m_k}+ic^\dagger_{-\uparrow m_k}c_{-\downarrow m_k}-ic^\dagger_{-\downarrow m_k}c_{-\uparrow m_k}\right) \\ &= -\tfrac{i}{2}\left(B_{12}-B_{21}-B_{34}+B_{43}\right) \end{aligned} \tag{44}$$

We retrieve all 15 of the SU(4) generators in the same way:

$$\begin{aligned} \mathcal{S}_x &= \tfrac{1}{2}\left(B_{12}+B_{21}+B_{34}+B_{43}\right) \\ \mathcal{S}_y &= -\tfrac{i}{2}\left(B_{12}-B_{21}+B_{34}-B_{43}\right) \\ \mathcal{S}_z &= \tfrac{1}{2}\left(B_{11}-B_{22}+B_{33}-B_{44}\right) \\ \\ T_x &= \tfrac{1}{2}\left(B_{13}+B_{31}+B_{24}+B_{42}\right) \\ T_y &= -\tfrac{i}{2}\left(B_{13}-B_{31}+B_{24}-B_{42}\right) \\ T_z &= \tfrac{1}{2}\left(B_{11}+B_{22}-B_{33}-B_{44}\right) \\ \\ N_x &= \tfrac{1}{2}\left(B_{12}+B_{21}-B_{34}-B_{43}\right) \\ N_y &= -\tfrac{i}{2}\left(B_{12}-B_{21}-B_{34}+B_{43}\right) \\ N_z &= \tfrac{1}{2}\left(B_{11}-B_{22}-B_{33}+B_{44}\right) \\ \\ \Pi_{xx} &= \tfrac{1}{2}\left(B_{14}+B_{41}+B_{23}+B_{32}\right) \\ \Pi_{yx} &= -\tfrac{i}{2}\left(B_{23}-B_{32}+B_{41}-B_{14}\right) \\ \Pi_{zx} &= \tfrac{1}{2}\left(B_{13}+B_{31}-B_{24}-B_{42}\right) \\ \Pi_{xy} &= -\tfrac{i}{2}\left(B_{32}-B_{23}+B_{41}-B_{14}\right) \\ \Pi_{yy} &= -\tfrac{1}{2}\left(B_{41}+B_{14}-B_{23}-B_{32}\right) \\ \Pi_{zy} &= -\tfrac{i}{2}\left(B_{31}-B_{13}-B_{42}+B_{24}\right). \end{aligned} \tag{45}$$

In this way, the SU(4) Lie algebra with the previous set of operators is written as a subalgebra of the SO(8) algebra of current consideration, using only linear combinations of the particle-hole operators.

6 Applications of the SO(8) Algebra: Collective Modes

Now that we have constructed an SO(8) Lie algebra for describing pair and particle-hole creation in the allowed states of grahene, we wish to use the model to understand the states that occur within a Landau level of graphene in a magnetic field, particularly when those electrons are highly correltated.

6.1 Degeneracies within the Landau level

Normally, we expect to see $2k+1$ degenerate levels within a single Landau level, where the possible momentum states range from $-k$ to k, which for a sample in a magnetic

field B corresponds to an electron degeneracy of

$$2\Omega_k = 2k+1 = \frac{BS}{(h/2e)},$$

where S is the area of the sample and $h/2e$ is the magnetic flux quantum. When we add in the additional 4 internal degrees of freedom that exist in graphene due to spin and isospin, and observe, as expected $4(2k+1)$ levels. If the level is half-filled, then we have $n = 2(2k+1)$ electrons, or $N = 2k+1$ electron pairs, and the pair density is

$$\frac{N}{S} = \frac{2B}{(h/2e)}$$

This discussion of degeneracies will serve us in determining the total number of electrons in each state we will describe.

6.2 Many-pair states and the highest-weight state

Using the six pair creation operators $A^\dagger_{ab}$, we can write down a state composed of these pairs as

$$(A^\dagger_{12})^{N_{12}}(A^\dagger_{13})^{N_{13}}(A^\dagger_{14})^{N_{14}}(A^\dagger_{23})^{N_{23}}(A^\dagger_{24})^{N_{24}}(A^\dagger_{12})^{N_{34}}|0\rangle, \tag{46}$$

where $|0\rangle$ represents the vaccuum state, that is to say, there are no electrons in the Landau level under consideration, and the levels below it are completely filled. The number of pairs created by each operator obey

$$N_{12}+N_{13}+N_{14}+N_{23}+N_{24}+N_{34} = N = \frac{n}{2}, \tag{47}$$

where n is the total number of electrons, and thus N is the number of pairs.

Referring to the commutation relations (42), we can see that the 16 particle-hole operators B_{ab} are closed under commutation, meaning that they generate a U(4) subalgebra of SO(8). In seeking the representations of the states in this representation, we first define the highest-weight state by considering all electrons to be in pairs created in the 1 and 2 states (with reference to (39), these are the $K\uparrow$ and $K\downarrow$ states). If we consider the half-filling ($2k+1$ pairs) of the Landau level, then this highest weight state can be written

$$\begin{aligned} |HW\rangle &= \tfrac{1}{(2k+1)!}\left(A^\dagger_{12}\right)^{2k+1}|0\rangle \\ &= \tfrac{1}{(2k+1)!}\left(\sum_{m_k} c^\dagger_{1m_k}c^\dagger_{2-m_k}\right)^{2k+1}|0\rangle, \end{aligned} \tag{48}$$

summed over the $2k+1$ values of m_k, from $-k$ to k. For the simplest case, this is not too hard to write out. We take $k=1$, then $m_k = (-1,0,1)$

$$\begin{aligned} |HW\rangle &= \tfrac{1}{3!}\left(c^\dagger_{1-1}c^\dagger_{21}+c^\dagger_{10}c^\dagger_{20}+c^\dagger_{11}c^\dagger_{2-1}\right)^3|0\rangle \\ &= \tfrac{1}{3!}\left(6c^\dagger_{1-1}c^\dagger_{21}c^\dagger_{10}c^\dagger_{20}c^\dagger_{11}c^\dagger_{2-1}\right)|0\rangle \\ &= \prod_{m_k=-k}^{m_k=k} c^\dagger_{1m_k}c^\dagger_{2-m_k}|0\rangle \end{aligned} \tag{49}$$

The key point here is that we have cancelled out every term in the expansion of the trinomial which contains any creation operator raised to a power higher than one, because otherwise the Pauli principle would be violated by having multiple electrons in the same state. In general, we can then show that the highest weight state can be written

$$|HW\rangle = \prod_{m_k=-k}^{m_k=k} c^\dagger_{1m_k} c^\dagger_{2-m_k} |0\rangle \tag{50}$$

6.3 States other than the highest weight state

To construct the other possible states in this subspace, we can apply the raising and lowering operators to the highest weight state. For example, let us look at the application of the valley isospin lowering operator T_- on the highest weight state.

$$\begin{aligned} T_- &\equiv \tfrac{1}{2}(T_x - iT_y) = \tfrac{1}{2}(B_{31} + B_{42}) \\ &= \frac{1}{2}\sum_{m_k} (c^\dagger_{3m_k} c_{1m_k} + c^\dagger_{4m_k} c_{2m_k}) \end{aligned} \tag{51}$$

Applying this to the highest weight state gives

$$\begin{aligned} |\psi\rangle &= T_-|HW\rangle = \tfrac{1}{2}(B_{31} + B_{42})|HW\rangle \\ &= \frac{1}{2}\prod_{m_k} \left(\sum_{n_k} \left(c^\dagger_{3m_k} c_{1m_k} + c^\dagger_{4m_k} c_{2m_k} \right) \right) c^\dagger_{1m_k} c^\dagger_{2-m_k} |0\rangle \\ &= \frac{1}{2}\prod_{m_k} \left(c^\dagger_{3m_k} c^\dagger_{2-m_k} - c^\dagger_{4-m_k} c^\dagger_{1m_k} \right) |0\rangle \end{aligned} \tag{52}$$

Here, we have used the fact that all terms cancel out except for those in which a creation operator is balanced exactly by an annihilation operator for the same state.

7 Coupled Representations

The electron creation and annihilation operators $c^\dagger$ and c defiined in Section 5 each carry a spin and a valley isospin, so the products $c^\dagger c^\dagger$, cc. and $c^\dagger c$ which correspond to the pair creation/annihilation and the particle-hole operators represent superpositions of states with indefinite spin and isospin, and so we refer to these representations as *uncoupled representations*.

If we wish to better understand the physical system, where spin is conserved in the absence of the Zeeman term, and isospin is conserved for low-energy excitations, we wish instead to use *coupled representations*, which give good, determined spin and isospin quantum numbers. To do so, we must refer to the Clebsch-Gordan coefficients, and write our new coupled representations as the sums of these coupling coefficients multiplied by the uncoupled representations.

7.1 Coupled representations of the pair creation/annihilation operators

For the pair creation operators, we can write the new coupled representations in the form

$$A^{\dagger TS}_{M_T M_S} \equiv \sum_{m_k} \sum_{m_1 m_2 n_1 n_2} C^{TM_T}_{\frac{1}{2}m_1\frac{1}{2}m_2} C^{SM_S}_{\frac{1}{2}n_1\frac{1}{2}n_2} c^\dagger_{m_1 n_1 m_k} c^\dagger_{m_2 n_2 m_k} \tag{53}$$

Here, S is the total spin and T is the total isospin of the pair, and M_S and M_T are their respective projections. The Clebsch-Gordan coefficients $C^{JM}_{j_1 m_1 j_2 m_2}$ couple (iso)spin vectors $\mathbf{j}_1 + \mathbf{j}_2 = \mathbf{J}$ to the possible projections $m_1 + m_2 = M$. Because the particles under consideration are electrons, which have spin $^1/_2$, the magnitude of each spin is $^1/_2$, and the possible values for total spin (or isospin, for the same reason) are 0 or 1. If the spin is 1, it can then have projection 1, 0, or -1, being one of the triplet states, or if the spin is 0, then it's projection is necessarily 0, and the pair is in the singlet state. Because of antisymmetry, the pair must be in either the $S = 0$, $T = 1$ (spin-singlet, isospin-triplet) or $S = 1, T = 0$ (spin-triplet, isospin singlet) state, or else the Pauli principle would be violated by having two electrons on the same site with the same spin.

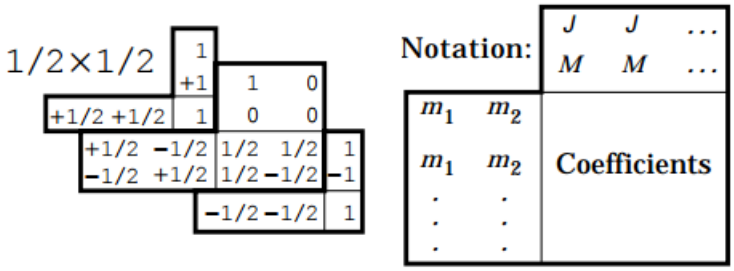

Figure 6: Clebsch-Gordan table for two spin-1/2 particles. Square roots are implied to be around each coefficient, and then any negative signs applied outside the square root.[16]

As an example, we can now calculate the operator $A^{\dagger 01}_{00}$, representing the isospin-singlet, spin-triplet configuration, where the spin projection is 0.

$$\begin{aligned}
A^{\dagger 01}_{00} &= \sum_{m_k} \sum_{m_1 m_2} \sum_{n_1 n_2} C^{00}_{\frac{1}{2}m_1\frac{1}{2}m_2} C^{10}_{\frac{1}{2}n_1\frac{1}{2}n_2} c^\dagger_{m_1 n_1 m_k} c^\dagger_{m_2 n_2 - m_k} \\
&= \sum_{m_k} C^{00}_{\frac{1}{2}\frac{1}{2}\frac{1}{2}-\frac{1}{2}} C^{10}_{\frac{1}{2}\frac{1}{2}\frac{1}{2}-\frac{1}{2}} c^\dagger_{K\uparrow m_k} c^\dagger_{K'\downarrow -m_k} + \sum_{m_k} C^{00}_{\frac{1}{2}\frac{1}{2}\frac{1}{2}-\frac{1}{2}} C^{10}_{\frac{1}{2}-\frac{1}{2}\frac{1}{2}\frac{1}{2}} c^\dagger_{K\downarrow m_k} c^\dagger_{K'\uparrow -m_k} \\
&\quad + \sum_{m_k} C^{00}_{\frac{1}{2}-\frac{1}{2}\frac{1}{2}\frac{1}{2}} C^{10}_{\frac{1}{2}\frac{1}{2}\frac{1}{2}-\frac{1}{2}} c^\dagger_{K'\uparrow m_k} c^\dagger_{K\downarrow -m_k} + \sum_{m_k} C^{00}_{\frac{1}{2}-\frac{1}{2}\frac{1}{2}\frac{1}{2}} C^{10}_{\frac{1}{2}-\frac{1}{2}\frac{1}{2}\frac{1}{2}} c^\dagger_{K'\downarrow m_k} c^\dagger_{K\uparrow -m_k} \\
&= \tfrac{1}{\sqrt{2}}\tfrac{1}{\sqrt{2}} A^\dagger_{14} + \tfrac{1}{\sqrt{2}}\tfrac{1}{\sqrt{2}} A^\dagger_{23} - \tfrac{1}{\sqrt{2}}\tfrac{1}{\sqrt{2}} A^\dagger_{32} - \tfrac{1}{\sqrt{2}}\tfrac{1}{\sqrt{2}} A^\dagger_{41} \\
&= A^\dagger_{14} + A^\dagger_{23}
\end{aligned} \tag{54}$$

Here, we have used the fact that if $M = 0$, then $m_1 = -m_2$ in any of our Clebsch-Gordan coefficients. We have also used the correspondence between spin/isospin values from (39), as well as the fact that $A^\dagger_{ab} = -A^\dagger_{ba}$. If we do this process for each of the

possible coupled combinations, we get the following:

$$A^{\dagger 10}_{00} = A^{\dagger}_{14} - A^{\dagger}_{23} \tag{55a}$$

$$A^{\dagger 10}_{10} = \sqrt{2}A^{\dagger}_{12} \tag{55b}$$

$$A^{\dagger 10}_{-10} = \sqrt{2}A^{\dagger}_{34} \tag{55c}$$

$$A^{\dagger 01}_{00} = A^{\dagger}_{14} + A^{\dagger}_{23} \tag{55d}$$

$$A^{\dagger 01}_{01} = \sqrt{2}A^{\dagger}_{13} \tag{55e}$$

$$A^{\dagger 01}_{0-1} = \sqrt{2}A^{\dagger}_{24}, \tag{55f}$$

and their respective Hermitian conjugates representing the coupled forms of the pair annihilation operators.

For normalization purposes, we choose to define instead a set of operators $S^{\dagger}$, $D^{\dagger}_{\mu}$ ($\mu = 0, \pm 1, \pm 2$), which are just the $A^{\dagger TS}_{M_T M_S}$ operators scaled by a factor of $\frac{1}{\sqrt{2}}$.

$$S^{\dagger} = \frac{1}{\sqrt{2}}A^{\dagger 10}_{00} = \frac{1}{\sqrt{2}}\left(A^{\dagger}_{14} - A^{\dagger}_{23}\right) \tag{56a}$$

$$D^{\dagger}_{2} = \frac{1}{\sqrt{2}}A^{\dagger 10}_{10} = A^{\dagger}_{12} \tag{56b}$$

$$D^{\dagger}_{1} = \frac{1}{\sqrt{2}}A^{\dagger 10}_{-10} = A^{\dagger}_{34} \tag{56c}$$

$$D^{\dagger}_{0} = \frac{1}{\sqrt{2}}A^{\dagger 01}_{00} = \frac{1}{\sqrt{2}}\left(A^{\dagger}_{14} + A^{\dagger}_{23}\right) \tag{56d}$$

$$D^{\dagger}_{-1} = \frac{1}{\sqrt{2}}A^{\dagger 01}_{01} = A^{\dagger}_{13} \tag{56e}$$

$$D^{\dagger}_{-2} = \frac{1}{\sqrt{2}}A^{\dagger 01}_{0-1} = A^{\dagger}_{24}, \tag{56f}$$

7.2 Coupled representations of the particle-hole operators

Now we use a similar method to couple the particle-hole operators B_{ab} to good possible operators which conserve spin and isospin. We define

$$P^{r}_{\mu} = \sum_{m_j m_l} (-1)^{\frac{3}{2}+m_l} C^{r\mu}_{\frac{3}{2}m_j \frac{3}{2}m_l} B_{m_j - m_l}. \tag{57}$$

Here, because the spin-isospin states are not independent, for the B operators, we have chosen to couple them to the projections of a fictitious angular momentum for a spin-3/2 particle m_i as follows:

$$\begin{array}{cccc} \tau & \sigma & a & m_i \\ + & \uparrow & 1 & {}^{3}/_{2} \\ + & \downarrow & 2 & {}^{1}/_{2} \\ - & \uparrow & 3 & {}^{-1}/_{2} \\ - & \downarrow & 4 & {}^{-3}/_{2} \end{array} \tag{58}$$

Then the normal particle-hole operators are

$$B_{m_j - m_l} = \sum_{m_k} c^{\dagger}_{m_j m_k} c_{-m_l m_k} - \frac{1}{4}\delta_{m_j - m_l}\Omega \tag{59}$$

This means that the possible values of r are $r = 0, 1, 2, 3$ and μ ranges from $-r$ to r, and the coefficients come from the ${}^{3}/_{2} \times {}^{3}/_{2}$ Clebsch-Gordan table, shown below.

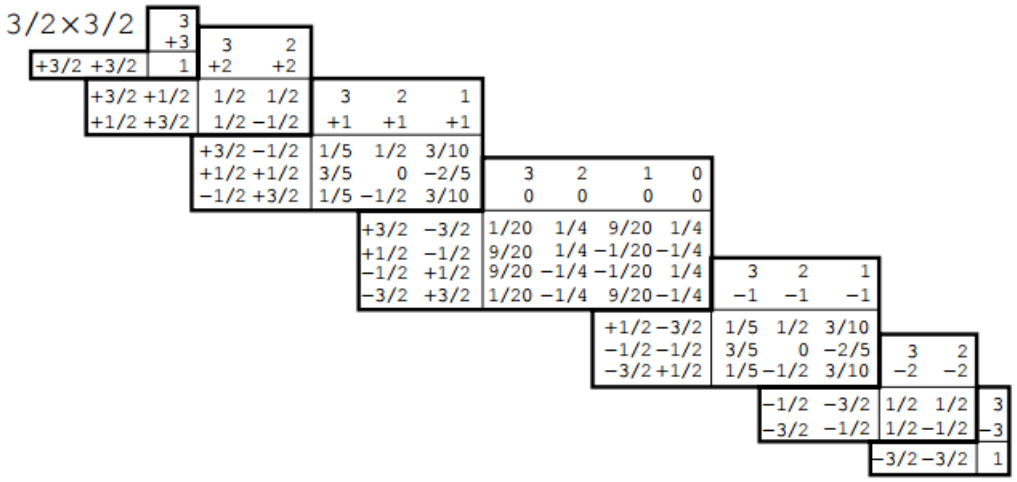

Figure 7: Clebsch-Gordan table for two spin-3/2 particles.[16]

As an example, we will calculate the operator P_2^2.

$$\begin{aligned} P_2^2 &= \sum_{m_j m_l} (-1)^{\frac{3}{2}+m_l} C^{22}_{\frac{3}{2} m_j \frac{3}{2} m_l} B_{m_j - m_l} \\ &= (-1)^2 C^{22}_{\frac{3}{2}\frac{3}{2}\frac{3}{2}\frac{1}{2}} B_{\frac{3}{2}-\frac{1}{2}} + (-1)^3 C^{22}_{\frac{3}{2}\frac{1}{2}\frac{3}{2}\frac{3}{2}} B_{\frac{1}{2}-\frac{3}{2}} \\ &= \frac{1}{\sqrt{2}} B_{13} + \frac{1}{\sqrt{2}} B_{24} \\ &= \frac{1}{\sqrt{2}} \left(B_{13} + B_{24}\right) \end{aligned} \tag{60}$$

If we do the same for all 16 possible combinations, we arrive at the following coupled

operators:

$$
\begin{array}{lll}
P^0_0 &= \frac{1}{2}\left(B_{11}+B_{22}+B_{33}+B_{44}\right) & \\
P^1_0 &= \sqrt{\frac{9}{20}}\left(B_{11}-B_{44}\right)+\sqrt{\frac{1}{20}}\left(B_{22}-B_{33}\right) & \\
P^1_1 &= -\sqrt{\frac{3}{10}}B_{12}-\sqrt{\frac{4}{10}}B_{23}-\sqrt{\frac{3}{10}}B_{34} & P^1_{-1} = \sqrt{\frac{3}{10}}B_{21}+\sqrt{\frac{4}{10}}B_{32}+\sqrt{\frac{3}{10}}B_{43} \\
P^2_0 &= \frac{1}{2}\left(B_{11}-B_{22}-B_{33}+B_{44}\right) & \\
P^2_1 &= \sqrt{\frac{1}{2}}\left(B_{34}-B_{12}\right) & P^2_{-1} = \sqrt{\frac{1}{2}}\left(B_{21}-B_{43}\right) \\
P^2_2 &= \sqrt{\frac{1}{2}}\left(B_{13}+B_{24}\right) & P^2_{-2} = \sqrt{\frac{1}{2}}\left(B_{31}+B_{42}\right) \\
P^3_0 &= \sqrt{\frac{1}{20}}\left(B_{11}-B_{44}\right)+\sqrt{\frac{9}{20}}\left(B_{33}-B_{22}\right) & \\
P^3_1 &= -\sqrt{\frac{1}{5}}B_{12}+\sqrt{\frac{3}{5}}B_{23}-\sqrt{\frac{1}{5}}B_{34} & P^3_{-1} = \sqrt{\frac{1}{5}}B_{21}-\sqrt{\frac{3}{5}}B_{32}+\sqrt{\frac{1}{5}}B_{43} \\
P^3_2 &= \sqrt{\frac{1}{2}}\left(B_{13}-B_{24}\right) & P^3_{-2} = \sqrt{\frac{1}{2}}\left(B_{31}-B_{42}\right) \\
P^3_3 &= -B_{14} & P^3_{-3} = B_{41}
\end{array}
\tag{61}
$$

We can also observe that the four operators B_{ii}, with $i = 1, 2, 3, 4$ are number operators of the form mentioned in Section 5.1, and we can choose to replace them by n_i, which denotes the number of electrons in state i, and the total number of particles is thus $n = n_1 + n_2 + n_3 + n_4$. We further observe that $P^0_0 = \frac{1}{2}(n - \Omega)$, and note that for undoped graphene at half-filling this will always be zero, because the degeneracy of the Landau level is the same as the number of pairs in the level (or half the number of electrons). In doped graphene, however, this will not be the case, and P^0_0 could offer a good way to describe how the doping changes the physics.

Because all of the 28 new coupled operators are merely linear combinations of the generators of our original SO(8) symmetry, they also form an SO(8) Lie algebra. However, the commutators become much more complicated in this form, and will not be explored here.

8 Inverse Transformations

Most of the preceding theoretical work is either well-established in the current graphene literature, or is currently under development by Drs. Guidry and Wu. My own involvement in the project has consisted of the creation of the dispersion relation figures 4 and 5, as well as checking the calculations related to the SO(8) symmetry, and correcting any errors. My other significant contribution has been the inverse transformation of the P^r_μ, presented above as a linear combination of the B_{ab}, to have the B_{ab} given as a combination of the P^r_μ, and then, using this, to write the original SU(4) operators in terms of P^r_μ. This work is presented below.

8.1 B_{ab} in terms of P^r_μ

First, we observe that, instead of needing to solve a 16×16 system of equations, the equations for the P^r_μ operators break down nicely into much smaller systems:

$$\begin{pmatrix} P^0_0 \\ P^1_0 \\ P^2_0 \\ P^3_0 \end{pmatrix} = \begin{pmatrix} \frac{1}{2} & \frac{1}{2} & \frac{1}{2} & \frac{1}{2} \\ \sqrt{\frac{9}{20}} & \sqrt{\frac{1}{20}} & -\sqrt{\frac{1}{20}} & -\sqrt{\frac{9}{20}} \\ \frac{1}{2} & -\frac{1}{2} & -\frac{1}{2} & \frac{1}{2} \\ \sqrt{\frac{1}{20}} & -\sqrt{\frac{9}{20}} & \sqrt{\frac{9}{20}} & -\sqrt{\frac{1}{20}} \end{pmatrix} \begin{pmatrix} B_{11} \\ B_{22} \\ B_{33} \\ B_{44} \end{pmatrix} \tag{62}$$

$$\begin{pmatrix} P^1_1 \\ P^2_1 \\ P^3_1 \end{pmatrix} = \begin{pmatrix} -\sqrt{\frac{3}{10}} & -\sqrt{\frac{4}{10}} & -\sqrt{\frac{3}{10}} \\ -\sqrt{\frac{1}{2}} & 0 & \sqrt{\frac{1}{2}} \\ -\sqrt{\frac{1}{5}} & \sqrt{\frac{3}{5}} & -\sqrt{\frac{1}{5}} \end{pmatrix} \begin{pmatrix} B_{12} \\ B_{23} \\ B_{34} \end{pmatrix} \quad \begin{pmatrix} P^1_{-1} \\ P^2_{-1} \\ P^3_{-1} \end{pmatrix} = \begin{pmatrix} \sqrt{\frac{3}{10}} & \sqrt{\frac{4}{10}} & \sqrt{\frac{3}{10}} \\ \sqrt{\frac{1}{2}} & 0 & -\sqrt{\frac{1}{2}} \\ \sqrt{\frac{1}{5}} & -\sqrt{\frac{3}{5}} & \sqrt{\frac{1}{5}} \end{pmatrix} \begin{pmatrix} B_{21} \\ B_{32} \\ B_{43} \end{pmatrix} \tag{63}$$

$$\begin{pmatrix} P^2_2 \\ P^3_2 \end{pmatrix} = \frac{1}{\sqrt{2}} \begin{pmatrix} 1 & 1 \\ 1 & -1 \end{pmatrix} \begin{pmatrix} B_{13} \\ B_{24} \end{pmatrix} \quad \begin{pmatrix} P^2_{-2} \\ P^3_{-2} \end{pmatrix} = \frac{1}{\sqrt{2}} \begin{pmatrix} 1 & 1 \\ 1 & -1 \end{pmatrix} \begin{pmatrix} B_{31} \\ B_{42} \end{pmatrix} \tag{64}$$

$$P^3_3 = -B_{14} \quad P^3_{-3} = B_{41}. \tag{65}$$

Each of these equations is in the simple form $\mathbf{a} = \mathbf{B}\mathbf{x}$, and can be easily solved by inversion of the coefficient matrix, giving $\mathbf{x} = \mathbf{B}^{-1}\mathbf{a}$. Doing so gives the following results:

$$\begin{aligned}
B_{11} &= \tfrac{1}{2}P^0_0 + \tfrac{3}{2\sqrt{5}}P^1_0 + \tfrac{1}{2}P^2_0 + \tfrac{1}{2\sqrt{5}}P^3_0 \\
B_{22} &= \tfrac{1}{2}P^0_0 + \tfrac{1}{2\sqrt{5}}P^1_0 - \tfrac{1}{2}P^2_0 - \tfrac{3}{2\sqrt{5}}P^3_0 \\
B_{33} &= \tfrac{1}{2}P^0_0 - \tfrac{1}{2\sqrt{5}}P^1_0 - \tfrac{1}{2}P^2_0 + \tfrac{3}{2\sqrt{5}}P^3_0 \\
B_{44} &= \tfrac{1}{2}P^0_0 - \tfrac{3}{2\sqrt{5}}P^1_0 + \tfrac{1}{2}P^2_0 - \tfrac{1}{2\sqrt{5}}P^3_0 \\
B_{12} &= -\sqrt{\tfrac{3}{10}}P^1_1 - \tfrac{1}{\sqrt{2}}P^2_1 - \tfrac{1}{\sqrt{5}}P^3_1 & B_{21} &= \sqrt{\tfrac{3}{10}}P^1_{-1} + \tfrac{1}{\sqrt{2}}P^2_{-1} + \tfrac{1}{\sqrt{5}}P^3_{-1} \\
B_{23} &= -\sqrt{\tfrac{2}{5}}P^1_1 + \sqrt{\tfrac{3}{5}}P^3_1 & B_{32} &= \sqrt{\tfrac{2}{5}}P^1_{-1} - \sqrt{\tfrac{3}{5}}P^3_{-1} \\
B_{34} &= -\sqrt{\tfrac{3}{10}}P^1_1 + \tfrac{1}{\sqrt{2}}P^2_1 - \tfrac{1}{\sqrt{5}}P^3_1 & B_{43} &= \sqrt{\tfrac{3}{10}}P^1_{-1} - \tfrac{1}{\sqrt{2}}P^2_{-1} + \tfrac{1}{\sqrt{5}}P^3_{-1} \\
B_{13} &= \tfrac{1}{\sqrt{2}}\left(P^2_2 + P^3_2\right) & B_{31} &= \tfrac{1}{\sqrt{2}}\left(P^2_{-2} + P^3_{-2}\right) \\
B_{24} &= \tfrac{1}{\sqrt{2}}\left(P^2_2 - P^3_2\right) & B_{42} &= \tfrac{1}{\sqrt{2}}\left(P^2_{-2} - P^3_{-2}\right) \\
B_{14} &= -P^3_3 & B_{41} &= P^3_{-3}
\end{aligned} \tag{66}$$

8.2 SU(4) generators in terms of the P^r_μ

Referring back to (5.2), where we wrote the 15 SU(4) generators in terms of the SO(8) B_{ab} operators, we can use this new information to now write them in terms of the coupled

P^r_μ operators as according to the transformation

$$\begin{aligned}
\mathcal{S}_x &= \sqrt{\tfrac{3}{10}}\left(P^1_{-1} - P^1_1\right) + \tfrac{1}{\sqrt{5}}\left(P^3_{-1} - P^3_1\right) \\
\mathcal{S}_y &= i\left(\sqrt{\tfrac{3}{10}}\left(P^1_1 + P^1_{-1}\right) + \tfrac{1}{\sqrt{5}}\left(P^3_1 + P^1_{-1}\right)\right) \\
\mathcal{S}_z &= \tfrac{1}{\sqrt{5}}P^1_0 + \tfrac{2}{\sqrt{5}}P^3_0 = n_1 - n_2 + n_3 - n_4 \\
T_x &= \tfrac{1}{\sqrt{2}}\left(P^2_2 + P^2_{-2}\right) \\
T_y &= -\tfrac{i}{\sqrt{2}}\left(P^2_2 - P^2_{-2}\right) \\
T_z &= \tfrac{4}{\sqrt{5}}P^1_0 - \tfrac{2}{\sqrt{5}}P^3_0 = n_1 + n_2 - n_3 - n_4 \\
N_x &= \tfrac{1}{\sqrt{2}}\left(P^2_{-1} - P^2_1\right) \\
N_y &= \tfrac{i}{\sqrt{2}}\left(P^2_{-1} + P^2_1\right) \\
N_z &= P^2_0 \\
\Pi_{xx} &= \tfrac{1}{2}\left(P^3_{-3} - P^3_3 + \sqrt{\tfrac{2}{5}}\left(P^1_{-1} - P^1_1\right) + \sqrt{\tfrac{3}{5}}\left(P^3_1 - P^3_{-1}\right)\right) \\
\Pi_{yx} &= \tfrac{i}{2}\left(P^3_{-3} + P^3_3 + \sqrt{\tfrac{2}{5}}\left(P^1_{-1} + P^1_1\right) - \sqrt{\tfrac{3}{5}}\left(P^3_1 + P^3_{-1}\right)\right) \\
\Pi_{zx} &= \tfrac{1}{\sqrt{2}}\left(P^3_2 + P^3_{-2}\right) \\
\Pi_{xy} &= \tfrac{i}{2}\left(P^3_{-3} + P^3_3 - \sqrt{\tfrac{2}{5}}\left(P^1_{-1} + P^1_1\right) + \sqrt{\tfrac{3}{5}}\left(P^3_1 + P^3_{-1}\right)\right) \\
\Pi_{yy} &= \tfrac{1}{2}\left(-P^3_{-3} + P^3_3 - \sqrt{\tfrac{2}{5}}\left(P^1_1 - P^1_{-1}\right) + \sqrt{\tfrac{3}{5}}\left(P^3_1 - P^3_{-1}\right)\right) \\
\Pi_{zy} &= -\tfrac{i}{\sqrt{2}}\left(P^3_{-2} - P^3_2\right).
\end{aligned} \tag{67}$$

9 Conclusion

In this paper, we have explored the unique structure of graphene, particularly its dispersion relation, which results in an isospin degeneracy and effectively massless electrons. We have examined the formation of Landau levels and the observed filling factors for the quantum Hall effect in graphene. Then, looking at the particular case of the $n = 0$ Landau level, we thoroughly investigated the currently used SU(4) symmetry model for low energy excitations, and the various ways in which it can be broken. Then, using fermion dynamical symmetry methods, we developed a new SO(8) symmetry out of electron-pair and electron-hole operators, which was shown to encompass the SU(4) model as well as allowing for additional possible states. The discussion of coupling allowed these states to be easier to physically interpret by following common conservation laws.

In fact, one of the primary reasons for converting to this new $\{S, S^\dagger_, D_\mu, D^\dagger_\mu, P^r_\mu\}$ basis is that it provides a correspondence to an SO(8) model used in a very different area of physics, which is nuclear structure physics. This is the Fermion Dynamical Symmetry Model, which provided an underlying basis for the widely-used, phenomological, interacting boson model[17]. This recognition allows for the graphene states to be analyzed in a new light, with the same group structure carried over from nuclear physics. Furthermore, though the systems are very different, the physical interpretations of the nuclear model may provide some insight into the physical interpretation of more complicated quantum Hall states in graphene. This is an area of ongoing research to which I have

now made my own small contribution, and which I hope to investigate in more detail in the future.

References

[1] K. S. Novoselov et al., Science **306**, 666 (2004).

[2] L.-A. Wu and M. Guidry, *SO(8) Fermion Dynamical Symmetry and Quantum Hall States in Graphene* (Unpublished).

[3] M. O. Goerbig, Rev. Mod. Phys. **83**, 1193 (2011).

[4] M. Guidry, *The Fractional Quantum Hall Effect in Graphene* (Lecture notes).

[5] K. von Klitzing, G. Dorda, M. Pepper, Phys. Rev. Lett. **45**, 494 (1980).

[6] D. C. Tsui, H. L. Stormer, and A. C. Gossard, Phys. Rev. Lett. **48**, 1599 (1982).

[7] L. Landau and E. Lifschitz, *Quantum Mechanics: Non-relativistic Theory*, 3rd. Ed (Butterworth-Heinemann, Oxford 1977) pp. 456-460.

[8] K. S. Novoselov et al, Nature **438**, 197 (2005).

[9] Y. Zhang et al, Nature **438**, 201 (2005).

[10] G. P. Jikitik and Y. V. Sharai, Phys. Rev. Lett. **82**, 2147 (1999).

[11] K. I. Bolotin, F. Ghahari, M. D. Shulman, H. L. Stormer, and P. Kim, Nature **462**, 196 (2009).

[12] X. Du, I Skachko, F. Duerr, A. Luican, and E. Y. Andrei, Nature **462**, 192 (2009).

[13] B. E. Feldman, B. Krauss, J. H. Smet, and A. Yacoby, Science **337**, 1196 (2012).

[14] M. Kharitonov, Phys. Rev. **B85**, 155439 (2012).

[15] F. Wu, I. Sodemann, Y. Araki, A. H. MacDonald, and T. Jolicoeur, Phys. Rev. **B90**, 235432 (2014) [arXiv:1406.2330].

[16] K. Hagiwara, Phys. Rev. **D66**, 010001 (2002).

[17] C.-L. Wu, D. H. Feng, X.-G. Cheng, J.-Q. Chen, and M. W. Guidry, Phys. Rev. **C36**, 1157 (1987).